

Quantifying the Cosmic Web I: The large-scale halo ellipticity-ellipticity and ellipticity-direction correlations

Jounghun Lee^{1*}, Volker Springel², Ue-Li Pen³, and Gerard Lemson²

¹*Department of Physics and Astronomy, FPRD, Seoul National University, Seoul 151-747, Korea*

²*Max-Planck-Institute for Astrophysics, Karl-Schwarzschild-Str. 1, D-85741 Garching, Germany*

³*Canadian Institute for Theoretical Astrophysics, Toronto, ON M5S, Canada*

Accepted 2007 ???. Received 2007 ???; in original form 2007 September 10

ABSTRACT

The formation of dark matter halos tends to occur anisotropically along the filaments of the Cosmic Web, which induces both ellipticity-ellipticity (EE) correlations between the shapes of halos, as well as ellipticity-direction (ED) cross-correlations between halo shapes and the directions to neighboring halos. We propose analytic fitting functions for the EE and the ED correlations in terms of the linear density correlation function, $\xi(r)$, based on the assumption that the filamentary distribution of the dark halos originates from the large-scale coherence of the initial tidal field. We also analyze the halo catalogue and the semi-analytic galaxy catalogue of the recent Millennium Simulation to measure the EE and ED correlations numerically at four different redshifts ($z = 0, 0.5, 1$ and 2). For the EE correlations, we find that (i) the major-axis correlation is strongest while the intermediate-axis correlation is weakest; (ii) the signal is stronger than the halo spin-spin correlations that exist at distances out to $10 h^{-1}\text{Mpc}$; (iii) the signal decreases as z decreases; (iv) and its behavior depends strongly on the halo mass scale, with larger masses showing stronger correlations at large distances. For the ED correlations, we find that (i) the correlations are much stronger than the EE correlations, and are significant even out to distances of $50 h^{-1}\text{Mpc}$; (ii) the signal also decreases as z decreases; (iii) and it increases with halo mass at all distances. Our analytic models are able to fit the numerical results very well in all cases. These results should be useful for quantifying the filamentary distribution of dark matter halos over a wide range of scales and to assess a possible systematic contamination of weak gravitational lensing signals.

Key words: methods:statistical – cosmology:theory – galaxies:clustering – galaxies:halos – large-scale structure of Universe

1 INTRODUCTION

One of the most striking features of the Universe is that the observed distribution of galaxies on large scales shows a web-like filamentary pattern, which is often called the “Cosmic Web”. Recent large N-body simulations of the cold dark matter cosmology demonstrated vividly the geometric richness of the filamentary web that spatially connects the dark matter halos, and which directly relates to the structure seen in the galaxy distribution. One of the most fundamental tasks in cosmology is thus to establish a physical model for the filamentary cosmic web and to quantitatively explain its global properties.

The existence of the filamentary web was originally predicted by the top-down scenario of the hot dark mat-

ter (HDM) model (Zel’dovich 1970). If cosmic structures form through top-down fragmentation, then one- and two-dimensional collapse of matter would naturally lead to the formation of sheet-like and filamentary structures on large scales. Therefore, it was regarded first as a mystery why and how the filamentary web came into being also in a cold dark matter (CDM) dominated universe.

A breakthrough was made by Bond et al. (1996) who developed an ingenious theory for the cosmic web that can explain the natural presence of a filamentary web in the CDM cosmogony. This cosmic web theory has provided a standard framework within which the formation of cosmic large-scale structure can be qualitatively understood. Yet, it is still quite difficult to describe the cosmic web quantitatively both in theoretical and in observational sides. Theoretically, the inherent anisotropic nature and geometrical complexity of the cosmic web makes it complicated to fully

* E-mail:jounghun@astro.snu.ac.kr

characterize its statistical properties. Observationally, it is hard to trace the filamentary structures from observational data, since there is no well-established way to identify them.

In spite of these difficulties, various methodologies and algorithms have already been suggested to quantify the filamentary structures: Higher-order N-point statistics has been used to describe the anisotropic matter distribution in a cosmic web (Croton et al. 2004; Kulkarni et al. 2007); the percolation statistics was used to characterize the filamentary shapes of the large-scale structures (Sahni et al. 1997; Shandarin & Yess 1998); the skeleton formalism has been developed to extract the filamentary structures from a three dimensional density field (e.g., Sousbie et al. 2007, and references therein); the Minimal-Spanning-Tree algorithm has been introduced to find the basic structural elements of the cosmic web (Colberg 2007).

Although the above methods are quite useful for determining the overall filamentary structure of the cosmic web, these approaches are largely phenomenological without accounting for the physical mechanism for the formation of the cosmic web. According to the theory proposed by Bond et al. (1996), the filamentary web originates from the large-scale coherence of the primordial tidal field, and its sharpening by nonlinear effects during structure growth. Part of this nonlinear sharpening effect arises from the gravitationally driven merging of halos and the infall of matter, which preferentially occurs along the most prominent filaments. This increases the anisotropy in the halo clustering and thus sharpens the filamentary web.

Hence, to describe the cosmic web quantitatively in terms of its underlying physical principles it will be necessary to account for the effects of the tidal field and the anisotropic merging along filaments. The tidal field causes intrinsic alignments of the principal axes of the dark halos in the cosmic web (Croft & Metzler 2000; Heavens et al. 2000; Catelan et al. 2001; Jing 2002; Hui & Zhang 2002; Lee & Pen 2007b), while anisotropic merging induces elongation of the major axes of the halos along prominent filaments (West 1989; West et al. 1991). As a result, there exist spatial correlations between the halo ellipticities (EE correlations), and cross-correlations between the halo ellipticities and the large-scale density field (ED cross-correlations). Hence, one can view the observed filamentary web as a large-scale manifestation of the EE and ED correlations, which are in turn induced by the effects of the tidal field and the anisotropic merging.

The goal of this paper is to quantify the filamentarity and the typical scales of the cosmic web in terms of the EE and ED correlations. This is also highly important for assessing to what degree these correlations can systematically bias weak gravitational lensing mass reconstructions and cosmological parameter estimates based on cosmic shear measurements. In fact, the ED cross-correlations have become a hot issue in the weak lensing community, since it has been realized that they could mimic weak lensing signals at a significant level (Hirata & Seljak 2004; Mandelbaum et al. 2006; Hirata et al. 2007).

The organization of this paper is as follows. In Section 2, we present physical models for the EE correlations and ED cross-correlations in the framework of linear perturbation theory. In Section 3, we describe the N-body dataset we use and explain how we measure halo ellipticities from the

N-body simulation and its associated galaxy catalogue. We then report numerical detections of the EE correlations and the ED cross-correlations in Sections 4 and 5, and examine how the signals depend on redshift and halo mass. Finally, in Section 6, we summarize the results and discuss the implications of our work.

2 PHYSICAL MODELS

According to the anisotropic merging model based on the cosmic web theory (West 1989; West et al. 1991; Bond et al. 1996), the gravitational collapse of forming dark matter halos occurs preferentially along filaments, which results in an elongation of the halo shapes in the direction of the local filament. Since the filaments represent the large-scale coherence of the linear tidal field, the dark halo ellipticities are expected to be aligned with the local tidal field.

Let $\hat{\mathbf{e}}_M \equiv (\hat{e}_i)$ represent a unit vector in the direction of the major axis of a dark matter halo with mass M , and let also $\hat{\mathbf{T}} \equiv (\hat{T}_{ij})$ be the linear tidal field with unit magnitude smoothed on the same mass scale M . An alignment of the halo's major axis with the local filament can be represented by $\hat{e}_i \hat{e}_j \propto \hat{T}_{ik} \hat{T}_{kj}$. In this linear model, the expected spatial ellipticity-ellipticity correlations (EE correlations) of halos can hence be described as a quadratic scaling of the two-point correlation function of the linear density field, $\xi_A^2(r)$, since the spatial correlations of the tidal field, $\hat{T}_{ik} \hat{T}_{kj}$, are well approximated as being proportional to $\xi^2(r)$ (Lee & Pen 2001). As $\xi^2(r)$ decreases rapidly with the separation distance r , the linear model predicts that the EE correlations exist only between close pairs with small separations.

The above expression, however, only provides a valid approximation if the density field (or equivalently, the tidal field) remains Gaussian, and if there is no nonlinear sharpening effect due to anisotropic infall/merging, as first pointed out by Hui & Zhang (2002). The nonlinear effect caused by anisotropic infall/merging and the development of non-Gaussianity in the density field will cause EE correlations at larger scales than expected based on linear theory. To model the large-scale EE correlations, it may therefore be necessary to express the EE correlations by several terms of the form $\xi^n(r)$ with $n < 2$. Very recently, Lee & Pen (2007b) have confirmed that the non-Gaussianity has a strong effect on the orientations of the galaxy spin vectors, whose spatial correlations are better described as $\xi(r)$ at low redshifts. Given that the ellipticities of the halos are affected not only by the non-Gaussianity but also by the anisotropic merging/infall, we expect that the scale of the EE correlations must be larger than that of the halo spin alignments.

Employing the quadratic function first suggested by Pen et al. (2000) for the spatial correlations of a unit vector, we define the halo EE correlation function, $\eta(r)$, as

$$\eta(r) \equiv \langle |\hat{\mathbf{e}}_M(\mathbf{x}) \cdot \hat{\mathbf{e}}_M(\mathbf{x} + \mathbf{r})|^2 \rangle - \frac{1}{3}, \quad (1)$$

where the constant $1/3$ is subtracted since $\langle |\hat{\mathbf{e}}_M(\mathbf{x}) \cdot \hat{\mathbf{e}}_M(\mathbf{x} + \mathbf{r})|^2 \rangle = 1/3$ when there is no correlation, so that we obtain $\eta(r) = 0$ in the absence of any correlation.

We suggest the following analytic fitting formula for $\eta(r)$:

$$\eta(r) \approx a_1 \tilde{\xi}_A^2(r) + a_2 \tilde{\xi}_A(r) + a_3 \tilde{\xi}_A^{1/2}(r), \quad (2)$$

where the three parameters a_1 , a_2 , a_3 , represent the correlation strengths at different (small and large) distances, and whose values are to be determined empirically. Since $\eta(r)$ is always positive and does not exceed $2/3$, the three parameters are in the range of $[0, 2/3]$. If there are no EE correlations, then all three parameters will be zero. If the EE correlations exist only on small scales, then a_1 will dominate, while if they are present at large scales, then a_2 and a_3 will dominate. Here, $\tilde{\xi}(r)_A$ is the *rescaled* auto-correlation function of the linear density field, defined as

$$\tilde{\xi}_A(r) \equiv \frac{\int P(k)[(\sin kr)/kr]W^2(k; M) d^3k}{\int P(k)W^2(k; M) d^3k}, \quad (3)$$

where $P(k)$ is the linear power spectrum, and $W(k; M)$ is the top-hat spherical filter corresponding to mass scale M . Note that $\tilde{\xi}(r=0) = 1$.

Although equation (2) was introduced to express the EE correlations of the major axis of halos, it can also be applied to the EE correlations of the intermediate and minor axes. In these cases, the values of the three correlation parameters are however expected to be lower than those for the major-axis case, since the physical cause of the correlations lies in the association of the major axes with the direction of the filament and of the anisotropic merging and infall.

In equation (2), it was assumed that the mass of both halos in the halo pair is the same. However, it is natural to expect that the correlations of the halo's major axes exist between different mass scales as well. Defining the cross-correlations of the major axes between the halos with different mass (say, M_1 and M_2) as

$$\eta_C(r) \equiv \langle |\hat{\mathbf{e}}_{M_1}(\mathbf{x}) \cdot \hat{\mathbf{e}}_{M_2}(\mathbf{x} + \mathbf{r})|^2 \rangle - \frac{1}{3}, \quad (4)$$

we suggest the following formula for $\eta_C(r)$, similar to equation (2):

$$\eta_C(r) \approx a_1 \tilde{\xi}_C^2(r) + a_2 \tilde{\xi}_C(r) + a_3 \tilde{\xi}_C^{1/2}(r) \quad (5)$$

where $\tilde{\xi}_C^2(r; R_1, R_2)$ is defined as

$$\tilde{\xi}_C(r) \equiv \frac{\int P(k)[\sin kr/kr]W(k; M_1)W(k; M_2) d^3k}{\int P(k)W(k; M_1)W(k; M_2) d^3k}. \quad (6)$$

We expect that the stronger the effect of the non-Gaussianity is, the stronger the cross-correlations $\eta_C(r)$ will be.

Another important correlation function for quantifying the cosmic web is the cross-correlation between the halo ellipticities and the large-scale density field. If the halo ellipticities are induced by the anisotropic infall and merging along the local filaments, then the orientations of the halo major axes must be preferentially aligned with the directions to the neighbouring halos. This effect can be measured in terms of ellipticity-direction (ED) cross-correlations of halo orientations and the location of halo neighbours.

We define the ED cross-correlations as

$$\omega(r) \equiv \langle |\hat{\mathbf{e}}_M(\mathbf{x}) \cdot \hat{\mathbf{r}}(\mathbf{x})|^2 \rangle - \frac{1}{3}, \quad (7)$$

where $\hat{\mathbf{r}} \equiv \mathbf{r}/r$ is a unit vector in the direction to a neighbouring halo at separation distance of r . We suggest the following fitting formula for $\omega(r)$, similar to equation (2):

$$\omega(r) \approx b_1 \tilde{\xi}_A^2(r) + b_2 \tilde{\xi}_A(r) + b_3 \tilde{\xi}_A^{1/2}(r) \quad (8)$$

where the three parameters b_1, b_2, b_3 lie in the range of $[-1/3, 2/3]$. For the case of the halo major-axis, the three parameters will have positive values, while for the cases of the halo minor or intermediate axes, the values of b_1, b_2, b_3 will be negative. We also expect that the values of b_1, b_2, b_3 will be larger than those of a_1, a_2, a_3 , since the ED cross-correlations are a more direct measure of the filamentary distribution of dark matter halos.

In the following two sections, we measure the EE correlations and ED cross-correlations by analyzing data from a recent high-resolution N-body simulation, and we determine the best-fit values of a_1, a_2, a_3 and b_1, b_2, b_3 at different redshifts.

3 SIMULATION DATA AND METHODOLOGY

Our analysis is based on the halo catalog and the semi-analytic galaxy catalog from the recent high-resolution *Millennium Simulation*¹, which followed 10^{10} dark matter particles in a Λ CDM concordance cosmology (Springel et al. 2005). The size of the periodic simulation box is $500 h^{-1} \text{Mpc}$ and each dark matter particle in the simulation has a mass of $8.6 \times 10^8 h^{-1} M_\odot$. The basic cosmological parameters of the simulation were chosen as $\Omega_m = 0.25$ (the mass density); $\Omega_\Lambda = 0.75$ (the vacuum energy density); $h = 0.73$ (the dimensionless Hubble constant); $\sigma_8 = 0.9$ (the linear power spectrum amplitude); and $n_s = 1$ (the slope of the primordial power spectrum).

As part of the analysis of the Millennium run, halos of dark matter particles were first identified with the standard friends-of-friends (FOF) algorithm, and then decomposed into gravitationally bound subhalos using the SUBFIND algorithm (Springel et al. 2001). Based on detailed merger trees constructed for the subhalos, the halos were then populated with luminous galaxy models using semi-analytic simulations of the galaxy formation process (Croton et al. 2006).

We here use the spatial distribution of subhalos and galaxies to characterize the shape of FOF halos, in analogy to the procedure applied to observational galaxy surveys (e.g., Mei et al. 2007). For each FOF halo, we locate the satellite galaxies belonging to it. Then, we measure their tensor (I_{ij}) of second order mass moments as

$$I_{ij} = \sum_{\alpha} m_{\alpha} x_{\alpha, i} x_{\alpha, j}, \quad (9)$$

where m_{α} is the luminosity (or, equivalently the stellar mass) of the α -th galaxy and \vec{x}_{α} is the position of the α -th galaxy measured from the center of the mass of the satellite galaxies. We restrict our analysis to FOF halos massive enough to contain more than five substructures.

By diagonalizing I_{ij} , we determine the three principal axes (major, intermediate, and minor axes) of I_{ij} . This allows us to measure the correlations between the three axes of the FOF halos as a function of separation. The results of our measurements are presented in detail in Section 4.

Before turning to our results, it is worth to discuss how

¹ The Millennium Simulation data are now available at <http://www.mpa-garching.mpg.de/millennium>

our methodology relates to other, previously applied methods to characterize the shape of halos. Note that we here do not use all dark matter particles of a FOF halo to measure I_{ij} . Instead, we only use the satellite galaxies (or substructures) as tracers of the shape. In general, measuring the shape of a halo is a somewhat ambiguous issue, where a number of different strategies have been applied in the literature, but no generally accepted standard procedure exists (see e.g. the discussion in Springel et al. 2004; Allgood et al. 2006). Part of the ambiguity in measuring halo shape stems from the fact that one cannot delineate the outer boundary of a halo in a clear-cut way. If all particles belonging to a FOF halo are used to measure I_{ij} , then the ellipticity of a halo may be overestimated because of the large weight of the most distant points on the major axis, while in contrast, if only those particles within a certain spherical radius are used to measure I_{ij} , then the ellipticity of the halo is likely underestimated.

We use satellite galaxies (or substructures) to measure I_{ij} , because this approach mimics observationally accessible procedures. We expect that this definition should give halo shapes similar to those measured with all dark matter particles, as substructure and galaxy density are tracers of the dark matter distribution (e.g., Agustsson & Brainerd 2006).

We will explicitly test this below. Note that we focus on quantifying the filamentary web induced by the anisotropic orientations of the halo ellipticities; we are not really interested in the *magnitude* of the shape distortion itself. This means that we are less sensitive to the details of measuring halo shape compared with attempts to quantify the axis ratio of the halo shape.

To examine to what extent different measuring methods yield different halo ellipticities, we carry out a simple test: Using a total of 227 FOF halos from the ‘milli’-Millennium simulation, which is smaller test run of the main Millennium simulation with a box size of $62.5 h^{-1} \text{Mpc}$ (Springel et al. 2005), we measured the halo shapes with three different methods: (A) using galaxies weighted by luminosity; (B) using dark matter substructures weighted by mass; and (C) using all dark matter particles. Then, we calculate the distribution of the angles θ between the principal axes of the halo shapes determined by these three methods. Figure 1 compares methods A and C (top), and methods B and C (bottom), in both cases plotting the histogram of the angles between the halos’ major, intermediate, and minor axes (left, middle, and right panels, respectively). As can be seen, there is a strong peak at $\theta = 0$, demonstrating that the halo principal axes obtained by the three different methods A, B and C are strongly correlated with one another. This correlation is particularly robust for the major axis, which defines the primary orientation of the predominantly prolate halos.

4 THE HALO ELLIPTICITY-ELLIPTICITY CORRELATION

Using the principal axes of the FOF halos from the Millennium simulation determined by the method described in Section 3, we first measure the EE correlations of the major, intermediate and minor axes separately as a function of the comoving distance r between two halo centers. We denote the three correlation functions as $\eta_I(r)$, $\eta_{II}(r)$, and

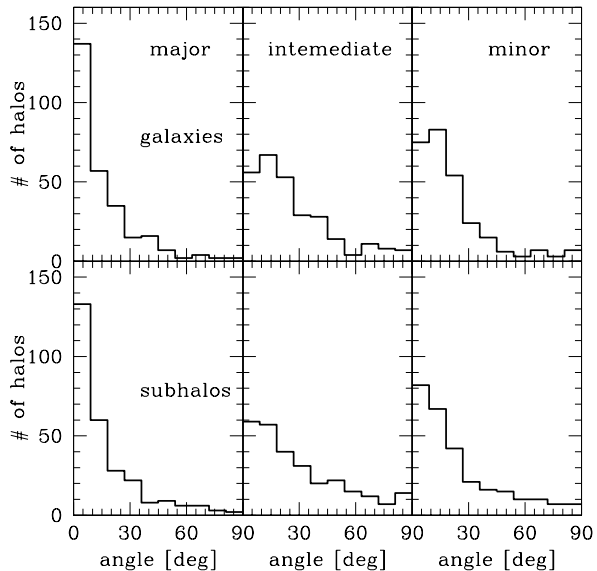


Figure 1. Distributions of the angles between the major, intermediate, and minor axes of the halos (left, middle, and right, respectively) from the milli-Millennium simulation, as determined by three different methods A, B, and C, which are based on the satellite galaxies, subhalos, and all particles belonging to the halos, respectively. The top-panels show the results from a comparison between the methods A and C, while the bottom panels give a comparison between the methods B and C.

$\eta_{III}(r)$, respectively. We also fit the physical model described by eqn. (2) to the numerical results by adjusting the three parameters a_1 , a_2 , and a_3 . The best-fit values of the three parameters are found through a χ^2 -minimization method (Bevington & Robinson 1996).

4.1 Evolution with redshift

In Figure 2, we show the three correlation functions measured at redshifts $z = 0, 0.5, 1$ and 2 in the top-left, top-right, bottom-left and bottom-right panels, respectively. In each panel, the red, blue and black lines represent the EE-correlations of the major, intermediate and minor axes of halos, respectively. The dotted line shows the expectation if there are no correlations. As can be seen, the major-axis correlations are strongest and the intermediate-axis correlations are almost zero at all redshifts.

Figure 3 compares the numerical results for the EE correlations of the halo major-axes with the analytic fitting model (red solid line) given by equation (2). In each panel, the errors for the numerical data points are estimated by the mean standard deviation for the case of no correlation: $\sigma_\eta \equiv 2/\sqrt{45N_{\text{pair}}}$, where N_{pair} is the number of halo pairs belonging to a given distance bin (Lee & Pen 2001).

For the calculation of the analytic model, we have employed the approximate formula given by Bardeen et al. (1986) for the Λ CDM power spectrum, using the same values of the cosmological parameters that were used for the Millennium run. For the shape factor Γ of the power spectrum parameterization, we adopted $\Gamma = \Omega_m h$. For the smoothing

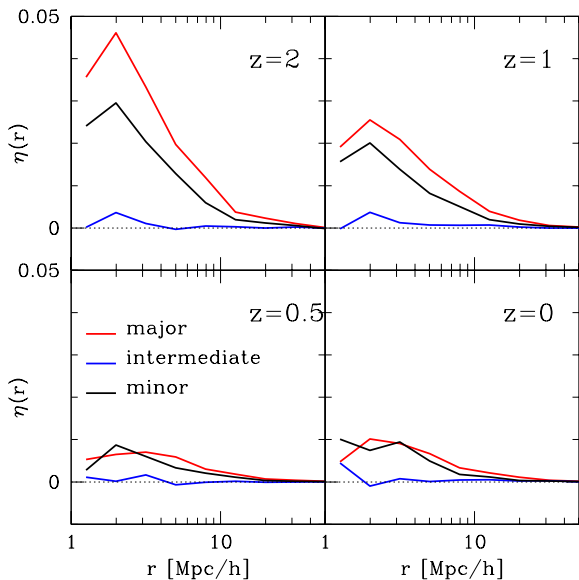


Figure 2. EE correlations of the halo major, intermediate, and minor axes (red, blue, and black lines) at four different redshifts: $z = 0, 0.5, 1,$ and 2 (top-left, top-right, bottom-left, and bottom-right, respectively).

mass scale in eq. (3), we use the mean mass \bar{M} averaged over the selected FOF halos.

Figure 3 reveals that the EE correlations of the halo major axes indeed exist at large distances out to $10 h^{-1} \text{Mpc}$. Our analytic model of eq. (2) is found to fit the numerical results quite well at all redshifts. The correlation is strongest at $z = 2$ and tends to decrease as z decreases. This might be due to the fact that the secondary infall and the growth of the less prominent filaments tend to randomize the directions of the halo major axes at low redshifts. Note, however, that the EE correlation is slightly stronger at $z = 0$ than at $z = 0.5$.

Table 1 lists the mean mass \bar{M} in unit of $10^{10} h^{-1} M_{\odot}$, the number of halos N_h , and the best-fit values of a_1 , a_2 , a_3 at four different redshifts z . As can be seen, the value of a_2 at $z = 1$ and 2 is an order of magnitude larger than the values of the other two parameters, implying that the EE correlations of the halo major axes are dominated by the term with a linear scaling of the density field at $z = 1$ and 2 .

Figure 4 plots the same measurements as Fig. 3 but for the EE correlations of the halo minor-axes. The analytic model fits the numerical results pretty well for this case as well. It is worth noting that at higher redshifts ($z = 2$ and 1), the minor-axis correlations are much weaker than the major-axis correlations, but at lower redshifts ($z = 0.5$ and 0) the major and the minor-axis correlations have almost the same strengths.

4.2 Variation with mass

In order to see how the correlation strength changes with halo mass, we consider four mass bins, each of which has about the same number of halos. Then, we measure the EE

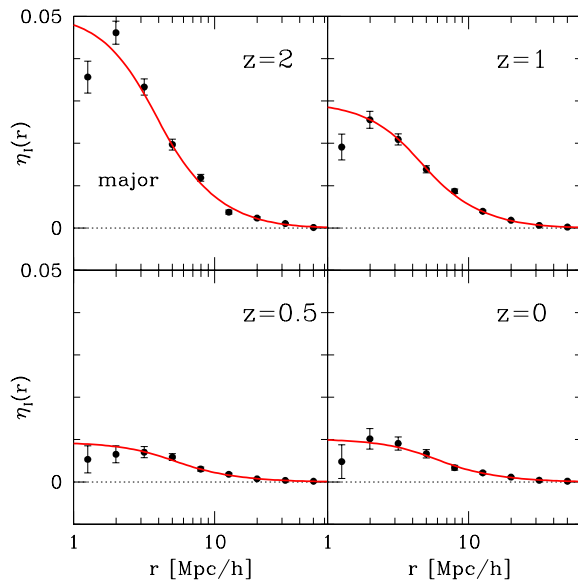


Figure 3. Comparison of the analytic fitting model (red solid line) with the numerical results (solid dots) for the EE correlations of the halo major axes at $z = 0, 0.5, 1$ and 2 .

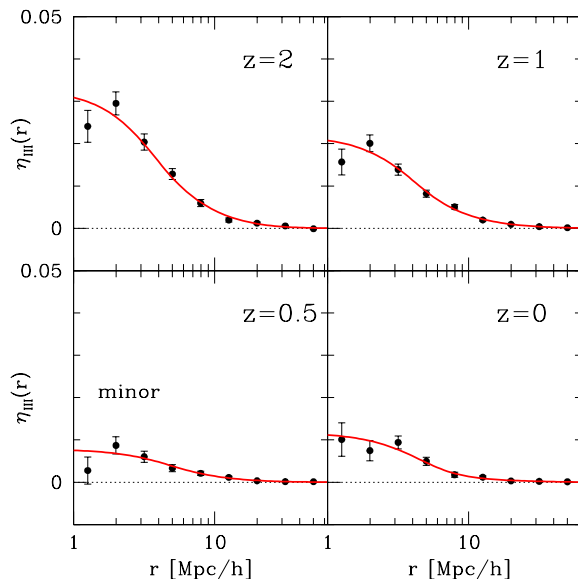


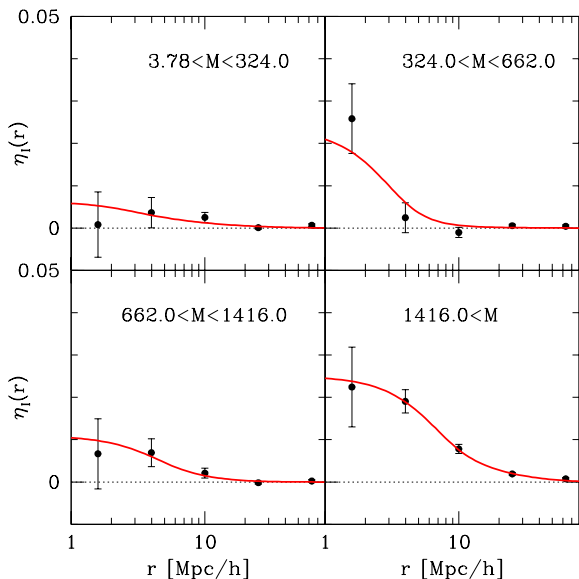
Figure 4. Same as Fig. 3 but for the case of the halo minor axes.

correlations of the halo major axes at each mass bin separately. Figure 5 plots the results and Table 2 lists the mass ranges of the bins and the resulting best-fit values of a_1 , a_2 , and a_3 .

As can be seen, the halo EE correlations strongly depend on the mass scale. For the mass bin 1 where the lowest mass halos belong, the EE correlation is negligible. For the mass bin 2 which correspond to the galactic halos with $M \sim 10^{12} h^{-1} M_{\odot}$, the EE correlation is found to be quite strong at small distance but negligible at distances larger

Table 1. Redshift (z), halo mean mass (\bar{M}) in unit of $10^{10} h^{-1} M_{\odot}$, number of halos (N_h), and the best-fit values of a_1 , a_2 and a_3 , for the EE correlations of the halo major axes.

z	\bar{M} [$10^{10} h^{-1} M_{\odot}$]	N_h	$a_1 \times 10^3$	$a_2 \times 10^3$	$a_3 \times 10^3$
0	1638.15	121773	5.16 ± 1.50	0.00 ± 0.88	5.16 ± 0.39
0.5	1118.823	131505	5.15 ± 1.43	0.00 ± 0.83	5.16 ± 0.35
1	810.92	125363	5.16 ± 1.56	20.63 ± 0.91	5.16 ± 0.38
2	448.33	73514	0.00 ± 2.55	46.41 ± 1.54	5.16 ± 0.68

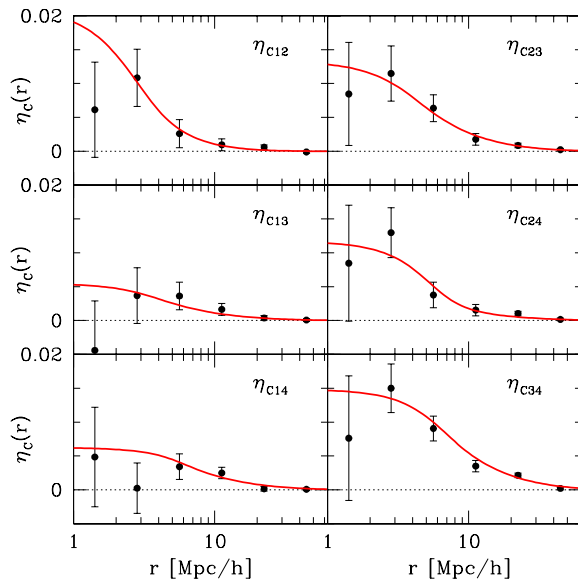
**Figure 5.** Comparison of the analytic fitting model (red solid line) with the numerical results (solid dots) for the EE correlations of the halo major axes at four different mass bins at $z = 0$. The mass bins have (almost) equal number of halos.

than a few Mpc. For the mass bin 3, the EE correlations are found to be weak at small distance but exist at large distances beyond a few Mpc at statistically significant level. For the mass bin 4, strong EE correlations are found at small distance and at large distances out to $10 h^{-1} \text{Mpc}$ as well. This suggests that the large-scale EE correlation becomes stronger as the halo mass increases.

According to the analytic fitting results shown in Table 2, the EE correlations of the galactic halos belonging to the mass bin 2 are well approximated as $\propto \xi_A^2(r)$ and decrease rapidly with r , suggesting that on this galactic mass scale the tidal fields provide a dominant contribution to the EE correlations. On the other hand, the EE correlation of the more massive halos belonging to the mass bin 3 behaves as $\propto \xi_A(r)$. This suggests that the effect of the non-Gaussianity in the density field and the anisotropic merging/infall make more important contribution for the massive halos belonging to the mass bin 3, generating the EE correlations at large distances. For the most massive halos belonging to the bin 4, the EE correlation behaves as $\propto \xi_A^2(r)$ on small scales and as $\propto \xi_A^{1/2}(r)$ on large scales, which suggests that both the strength and the scale of the EE correlation increase as the

Table 2. bin ID, the mean halo mass (\bar{M}) in unit of $10^{10} h^{-1} M_{\odot}$, and the best-fit values of a_1 , a_2 and a_3 , for the EE correlations of the halo major axes at $z = 0$.

bin ID	\bar{M} [$10^{10} h^{-1} M_{\odot}$]	$a_1 \times 10^3$	$a_2 \times 10^3$	$a_3 \times 10^3$
1	185.03	0.00 ± 11.10	0.00 ± 5.94	5.16 ± 2.13
2	478.32	25.78 ± 8.61	0.00 ± 4.70	0.00 ± 1.81
3	969.26	0.00 ± 6.69	10.31 ± 3.78	0.00 ± 1.58
4	4914.35	15.47 ± 3.70	0.00 ± 2.22	10.31 ± 1.11

**Figure 6.** Comparison of the analytic fitting model (red solid line) with the numerical results (solid dots) for the EE cross-correlations of the halos between different mass bins at $z = 0$.

hierarchical structure formation proceeds along anisotropic filaments.

We have also measured the cross-correlations of the major axes between halos belonging to different mass bins. Figure 6 shows these cross-correlations and compares the numerical results with the analytic fitting model of eq. (5). Here η_{Cij} represents the cross-correlations between the mass bin i and j listed in Table 2, where $i, j \in [1, 4]$. As can be seen, there exist significant cross-correlations between the neighbouring mass bins 1 and 2, 2 and 3, as well as 3 and 4.

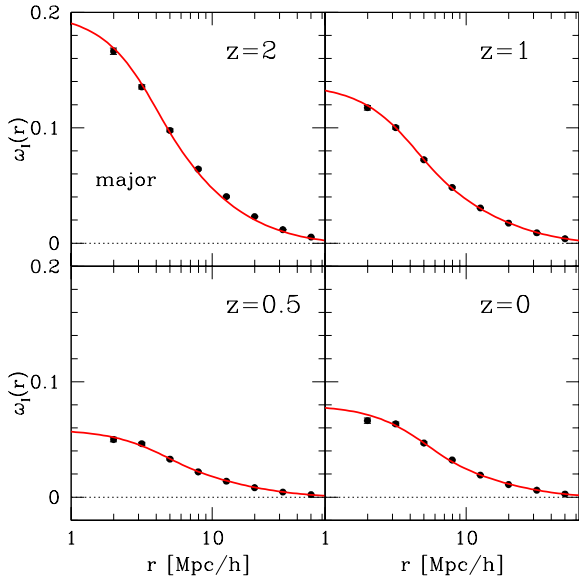


Figure 7. Comparison of the analytic fitting model (red solid line) with the numerical results (solid dots) for the ED correlations of the halo major axes at $z = 0, 0.5, 1$ and 2 .

Table 3. The best-fit values of the three correlation parameters for the ED correlations of the halo major axes.

z	$b_1 \times 10^3$	$b_2 \times 10^3$	$b_3 \times 10^3$
0	25.78 ± 1.61	0.00 ± 0.90	51.56 ± 0.37
0.5	15.47 ± 1.56	0.00 ± 0.85	41.25 ± 0.33
1	36.09 ± 1.75	15.47 ± 0.94	87.66 ± 0.37
2	36.09 ± 3.09	36.90 ± 1.66	128.91 ± 0.66

5 THE ELLIPTICITY-DIRECTION CROSS CORRELATIONS OF HALOS

We have also measured the ED correlations between the halo major, intermediate and minor axes and the unit vectors in the directions to neighbouring halos, as a function of the comoving distance r between the halo centers. The three correlation functions are denoted as $\omega_I(r)$, $\omega_{II}(r)$, and $\omega_{III}(r)$, respectively. Fitting the physical model of eq. (8) to the numerical results, we determine the best-fit values of b_1 , b_2 , b_3 , again with the help of a χ^2 -statistics.

5.1 Evolution with redshift

In Figure 7, we show ω_I at redshifts $z = 0, 0.5, 1$ and 2 . Since we are mainly in the cross-correlations between the halo principal axes and the large scale density field here, we focus on separation scale greater than $1h^{-1}\text{Mpc}$. Table 3 lists the best-fit values of b_1 , b_2 , and b_3 for these cases. As can be seen, the ED correlations of the halo major axes are much stronger than the EE correlations shown in Fig. 3. The ED signal is statistically significant even at distances out to $50h^{-1}\text{Mpc}$. Our analytic model of eq. (8) is again able to fit the numerical results very well.

The ED correlations for the intermediate and minor axes of halos, ω_{II} and ω_{III} , are plotted for redshifts $z = 0,$

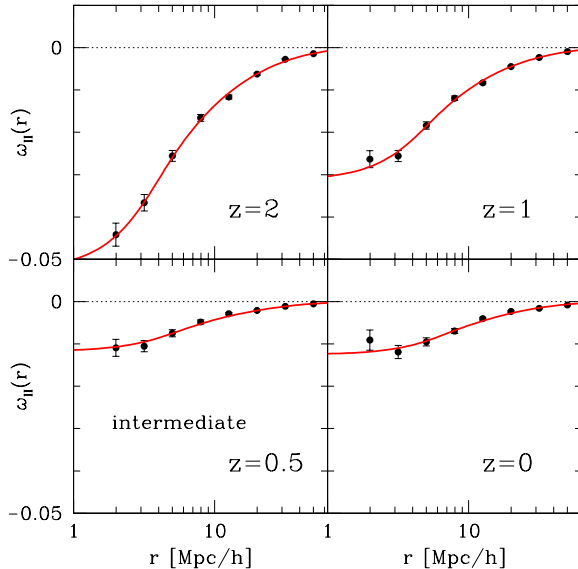


Figure 8. Same as Fig. 7 but for the case of the halo intermediate axes.

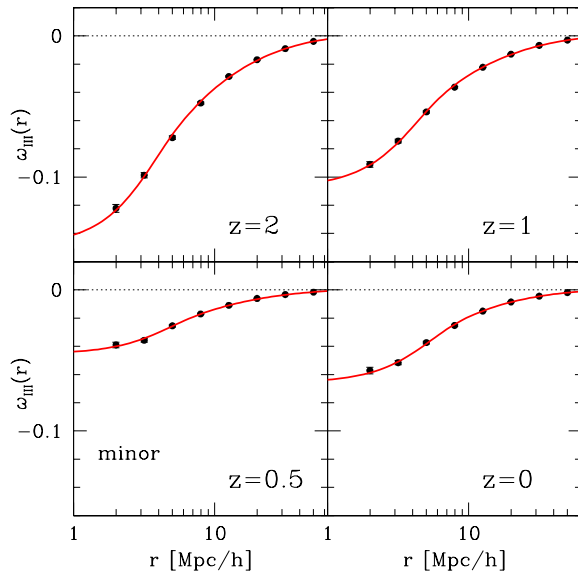


Figure 9. Same as Fig. 7 but for the case of the halo minor axes.

$0.5, 1$ and 2 in Figs. 8 and 9, respectively. As expected, the intermediate and minor axes are *anti-correlated* with the directions to neighbouring halos. These results demonstrate clearly that the halo major axes preferentially point in the directions where the local density stays high, hence this gives a quantitative measure for the filamentary distribution of the halos in the cosmic web.

Finally, we have also investigated how the ED cross-correlations vary with the halo mass scale. Figure 10 compares the numerical results with the analytic fitting model, and Table 4 lists the best-fit values of the three correlation parameters. As can be seen, the ED cross-correlations be-

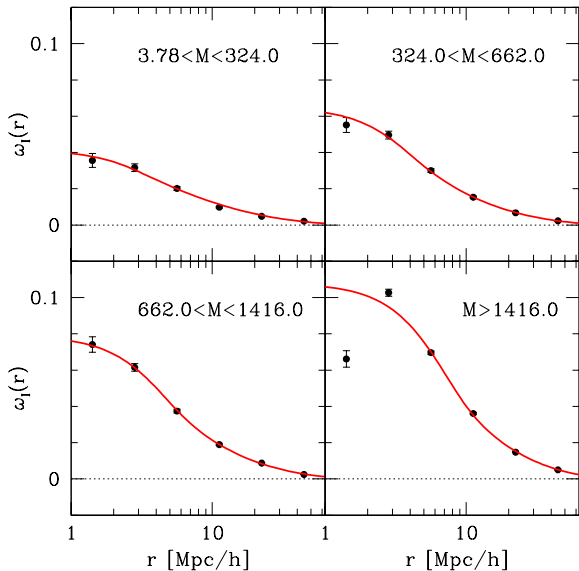


Figure 10. ED cross-correlations of the major axes at $z = 0$ as a function of halo mass scale.

Table 4. Analytic fit parameters of the ED cross-correlations shown in Fig. 10, as a function of mass scale.

M	$b_1 \times 10^3$ $10^{10} h^{-1} M_\odot$	$b_2 \times 10^3$	$b_3 \times 10^3$
185.03	0.00 ± 4.33	0.00 ± 2.28	41.41 ± 0.77
478.32	0.00 ± 3.28	20.03 ± 1.81	41.25 ± 0.66
969.26	20.62 ± 2.63	10.31 ± 1.49	46.41 ± 0.58
4914.35	46.41 ± 1.53	0.00 ± 0.92	61.88 ± 0.42

come stronger in higher mass-bins. This indicates that the anisotropic merging/infall contributes significantly to the ED cross-correlations.

6 SUMMARY AND DISCUSSION

In this work, we have proposed a physically motivated analytic fitting model for the halo ellipticity-ellipticity (EE) correlation function, characterized by three free parameters, a_1 , a_2 and a_3 . These three parameters represent the amplitudes of three terms which are proportional to $\xi_A^2(r)$, $\xi_A(r)$ and $\xi_A^{1/2}(r)$, respectively, where $\xi_A(r)$ is the filtered linear density two-point correlation function.

By analyzing the halo data and the semi-analytic galaxy catalog from the Millennium simulations at $z = 0, 1, 0.5$ and 2 , we have measured the EE correlations and determined the best-fit values of a_1 , a_2 and a_3 . We found that the EE correlations of the halo major axes are stronger than the halo spin-spin correlations measured by Lee & Pen (2007a). At the smallest distance bin, they are close to 0.03 and remain significant at distances out to $10 h^{-1}$ Mpc. The EE correlations are found to be strongest for the case of the halo major axes, and weakest for the case of the intermediate axes. We also found that the EE correlations of all three axes decrease as z decreases. This might be due to the growth of secondary

filaments at low redshifts and the beginning ‘freeze-out’ of structure growth in Λ CDM, which plays a role in randomizing the halo ellipticities.

In addition, the EE correlation function shows a strong dependence on halo mass. On the galactic halo scale, it behaves as $\propto \xi_A^2(r)$, while on the cluster halo scale, it is approximated as $\propto \xi_A^{1/2}(r)$ on the large scale. However, best-fits to the numerical results are obtained only when all three terms in the analytic model are included.

We also calculated EE correlations between halos belonging to different mass bins. Our results show that EE cross-correlations between neighboring mass bins exist at a statistically significant level as well.

We have also suggested a similar analytic model for the cross-correlations between the halo principal axes and the directions to neighbouring halos (ED), characterized in an analogous way by three free parameters, b_1 , b_2 and b_3 . We have measured the ED cross correlations by using the numerical data from the Millennium simulation and found that the ED cross-correlations are much stronger than the EE correlations, at all distances. Remarkably, they are detected even at distances out to $50 h^{-1}$ Mpc at a statistically significant level. The ED cross-correlation decrease as z decreases and increase as the halo mass M increases, suggesting a dominant role of anisotropic merging and infall of matter in establishing these correlations. We find that the intermediate and the minor axes of the halos are anti-correlated with the directions to the neighbouring halos, which is consistent with an alignment of the halos shape with the orientation of the local filament.

The EE correlations and the ED cross-correlations that we have measured here provide a useful tool to statistically characterize the anisotropy and the relevant scales of the cosmic web. Since these correlations are very well described by the physically motivated three-parameter fitting function we proposed, our results for the EE correlations and the ED cross-correlations can be concisely summarized in terms of 3×3 matrices, whose components are the fitting parameters for each of the 3 principal axes. The matrix effectively measures the degree of filamentarity and the scale of the cosmic web, depending on which components have higher values. It will be interesting to compare the results we obtained here for the Λ CDM cosmology with observational data from large galaxy redshift surveys. This will in general require also a modelling of redshift space distortions.

Another important application of our result lies in studies of weak gravitational lensing. The issue of a potential cross-correlation between galaxy ellipticities and the weak gravitational lensing shear (GI cross-correlations) was first raised by Hirata & Seljak (2004). They claimed that if such GI cross-correlations exist, then they would affect the weak lensing signal as another systematic contaminant whose effect is hard to control. The GI cross-correlations are expected to occur primarily due to the ED cross-correlations: If the intrinsic ellipticities of the galaxies are cross-correlated with the surrounding large-scale density field, then it will in turn lead to a cross-correlation between the gravitational lensing shear and the galaxy ellipticities. Recent observations indeed have reported detections of the GI correlation signals in low-redshift Galaxy surveys (Mandelbaum et al. 2006; Hirata et al. 2007).

The quantitative physical model for the ED cross-

correlations provided here should be useful in controlling the systematics due to GI cross-correlations in weak lensing searches. In future work, we plan to investigate in detail the relation between the observed GI cross-correlations and the ED cross-correlations of the cosmic web.

ACKNOWLEDGMENTS

The Millennium Simulation analyzed in this paper was carried out by the Virgo Supercomputing Consortium at the Computing Centre of the Max-Planck Society in Garching, Germany. We thank S.D.M. White for stimulating discussion. J.L. is very grateful to the warm hospitality of S.D.M. White and the Max Planck Institute for Astrophysics (MPA) in Garching where this work was initiated and performed. J.L. acknowledges financial support from Korea Science and Engineering Foundation (KOSEF) grant funded by the Korean Government (MOST, NO. R01-2007-000-10246-0).

REFERENCES

- Agustsson I., Brainerd T. G., 2006, *ApJ*, 644, L25
 Allgood B., et al., 2006, *MNRAS*, 367, 1781
 Atlay G., Colberg J. M., Croft R. A. C., 2006, *MNRAS*, 1422, 1428
 Bardeen J. M., Bond J. R., Kaiser N., Szalay, A. S., 1986, *ApJ*, 304, 15
 Bevington P. R., Robinson D. K., 1996, *Data Reduction and Error Analysis for the Physical Sciences* (Boston : McGraw-Hill)
 Bond J., R., Kofman L., Pogosyan D., 1996, *Nature*, 380, 603
 Catelan P., Kamionkowski M., Blandford R. D., 2001, *MNRAS*, 320, L7
 Colberg J. M., 2007, *MNRAS*, 375, 337
 Crittenden R. G., Natarajan P., Pen U. L., Theuns T., 2001, *ApJ*, 559, 552
 Crittenden R. G., Natarajan P., Pen, U. L., Theuns, T., 2002, *ApJ*, 568, 20
 Croft R. A. C., Metzler C. A., 2000, *ApJ*, 545, 561
 Croton D. J., et al. 2004, *MNRAS*, 352, 1232
 Croton D. J., Springel V., White S. D. M., De-Lucia G., Frenk C. S., Gao L., Jenkins A., Kauffmann G., Navarro J. F., Yoshida N., 2006, *MNRAS*, 365, 11
 Heavens A., Refregier A., Heymans C. 2000, *MNRAS*, 319, 649
 Hirata, C. M., Seljak U., 2004, *PRD*, 70, 063526
 Hirata C. M. et al., 2004, *MNRAS*, 353, 529
 Hirata C. M. et al., 2007, preprint [astro-ph/0701671]
 Hui L., Zhang Z., 2002, preprint [astro-ph/0205512]
 Jing Y., 2002, *MNRAS*, 335, L89
 Kulkarni G. V., Nichol R. C., Sheth R. K., Seo H. J., Eisenstein D. J., Gray A. 2007, *MNRAS*, 378, 1196
 Lee J., Kang X., Jing Y., 2005, *ApJ*, 629, L5
 Lee J. Pen U. L., 2000, *ApJ*, 532, L5
 Lee J., Pen U. L., 2001, *ApJ*, 555, 106
 Lee J., Pen U. L., 2002, *ApJ*, 567, 111
 Lee J., Pen U. L., 2007a, preprint [arXiv:0707.1690]
 Lee J., Pen U. L., 2007b, preprint [arXiv:0707.3232]
 Mandelbaum R., Hirata C. M., Ishak M., Seljak U., Brinkmann J., 2006, *MNRAS*, 367, 611
 Mei S., et al., 2007, *ApJ*, 655, 144
 Mo H. J., Mao S., White S. D. M., 1998, *MNRAS*, 295, 319
 Navarro J. F., Abadi M.G., Steinmetz M., 2004, *ApJ*, 613, L41
 Patiri S. G., Cuesta A. J. Prada, F., Betancort-Rijo, J., Klypin A., 2006, *ApJ*, 652, 75
 Pen U. L., Lee J., Seljak U., 2000, 543, L107
 Shandarin S. F., Yess C., 1998, *ApJ*, 505, 12
 Sahni V., Sathyaprakash B. S., Shandarin S. F., 1997, *ApJ*, 476, L1
 Sousbie T., Pichon C., Colombi S., Novikov D., Pogosyan D., 2007, *MNRAS*, 657, 30
 Springel V. et al., 2001, *MNRAS*, 328, 726
 Springel V., White S.D.M., Hernquist L., 2004, *IAU Symposium 220*, Eds. S.D. Ryder et al., San Francisco: Astronomical Society of the Pacific, p. 421
 Springel V. et al., 2005, *Nature*, 435, 629
 West M. J., 1989, *ApJ*, 347, 610
 West M. J., Willumsen C., Dekel A., 1991, *ApJ*, 369, 287
 White S. D. M., 1984, *ApJ*, 286, 38
 Zel'dovich Y. B. 1970, *A&A*, 5, 84

This paper has been typeset from a \TeX / \LaTeX file prepared by the author.